MULTI-IMAGE MATCHING FOR
AUTOMATIC OBJECT RECONSTRUCTION

Juliang SHAO and Clive FRASER
Department of Geomatics
The University of Melbourne
Parkville, 3052
Australia
Email: jsha@sli.unimelb.edu.au

Commission V, Working Group V/1

ABSTRACT

This paper deals with automatic reconstruction of a digital multi-ray photogrammetric network, which comprises multiple nodes, each node indicating one object point and its corresponding multiple imaging rays. In the automatic reconstruction, a novel multi-image matching (MIM) technique including consecutive consideration of all images as reference images is proposed. The MIM comprises three phases. The first is an establishment of the relationship between seed points in one image and multiple matching candidates in the overlapping images. This is carried out by a combined utilisation of epipolar curve chains, similarity measures and range constraints, and leads to the initial reconstruction of the multi-ray network. The second phase involves the creation of geometric relationships among compatible, neighbouring feature points in the same image via local consistency verification. These relationships contribute to a global matching quality control using a relaxation process. The global quality control in turn leads to a refined multi-ray network reconstruction which employs a check for correspondence ambiguities. The reported MIM technique is distinct from alternative matching approaches in pure image space or object space which have appeared in the literature. As opposed to least-squares matching where three dimensional coordinate vectors associated with many other parameters are combined via collinearity equations for repeatedly approaching the optimal points and especially for very high precision correlation, with this approach multi-ray triangulation residuals in object space are still employed, but only to remove ambiguities among multiple candidate feature points. In the proposed strategy, matching accuracy is enhanced by sub-pixel interest point extraction and multi-ray triangulation. The matching speed in the multi-ray network reconstruction in the case of four close-range images reaches 115 3D points per second on a Pentium-200 PC. The resulting accuracy approaches 0.1 pixels.

1. INTRODUCTION

Traditionally, aerial photogrammetric blocks of photography exhibit a regular 60% forward, and either 20-30% or 60% side overlap. With the recent application of high-resolution digital still video cameras to local area mapping, however, practical considerations and the desire to enhance accuracy and reliability in subsequent block triangulation have led to the introduction of multi-image coverage with a more irregular geometry (e.g. Maas, 1996). This irregular coverage is even more pronounced in digital close-range photogrammetry and machine vision where convergent imaging configurations coupled with complex object shapes lead to inhomogenous distributions of multi-ray intersections. This paper discusses the subject of automatic object reconstruction from a multi-image network, where the imaging configurations can be either regular or irregular in terms of both 'overlap' and the number of rays intersecting at each object point. The network can be thought of as comprising multiple nodes, with each node indicating an object point and 2 to n imaging rays, where n is the total number of images. The multi-image matching (MIM) technique involves the reconstruction of the multi-ray network through the matching of extracted feature points and thus must be viewed in the context of a method of solution for the image point correspondence problem. It is a feature-based, rather than intensity-based approach, which considers all possible imaging rays to a particular feature point.

Research into MIM has recently been active in aerial and close-range photogrammetry, and in computer vision, since the technique has the following favourable matching properties: *robustness, occlusion avoidance* and *high accuracy*. There are reported strategies for handling trinocular vision [e.g. Chiou, Chen, Hung and Lee, 1995; Faugeras, Lustman and Toscani, 1987; Ito and Ishii, 1986; Shibasaki and Murai, 1988; Wu and Murai, 1997] and an abundant number of techniques for undertaking motion sequences. The trinocular methods are much more stable than their binocular counterparts because of additional similarity measure constraints and extra epipolar geometric constraints from the third camera station, assuming the centers of the projection of the three camera stations are non-collinear. However, these algorithms can generally not be directly adapted for the case of more than three camera stations and hence they will not be further considered. Also, the matching techniques in motion sequences are based on tracking due to the presence of abundant sets of constraints.

On the other hand, the determination of image correlation from a set of widely-spaced views is a challenging issue. A number of algorithms for MIM have been proposed in recent years [e.g. Collins, 1996; Gruen and Baltsavias, 1988; Heipke, 1992; Maruya, Nemoto and Takashima, 1992; Okutomi and Kanade, 1993; Maas, 1996], with each being motivated by one or more specific tasks which preclude general judgement as to whether they are "good" or "bad". The goal of designing a more general strategy for MIM, oriented to a broad range of applications, is pursued in this paper.

The foundations of MIM with geometrical constraints were laid down by Gruen and Baltsavias (1988). In this technique the

fundamental computational strategy is to employ least-squares estimation for the iterative determination of homologous points. The highlights of the approach are very high accuracy of correlation through the introduction of a variety of parameters, such as interior and exterior orientation elements, image feature parameters, model correction parameters, individual object space coordinates and a digital surface model, into the least-squares model. In contrast to these beneficial characteristics, the well-known drawbacks are the need for more accurate initial values and the very high computational effort involved. The least-squares MIM approach is often too slow to warrant practical use. Heipke (1992) has also followed a least-squares approach for MIM, which emphasises correlation in object space. However, with this approach significant optimisation problems arise due to the large number of parameters carried and the requirement for accurate initial values.

A common MIM problem is the selection of an image as a fixed "reference" image. Features and/or intensity templates are specified on the reference image, and then a search is made for correspondences on the other images via certain constraints. However, if important features are missing in the reference image due to mis-extraction or occlusion, the matching possibilities of these corresponding object points are lost. Although the problem can be solved by an extension that repeatedly captures another image as a reference, the significant computation time of the least-squares approach limits the practicability of this extension.

An image to object back-projection mechanism has been proposed to simplify the matching procedure [Collins, 1996]. This approach assumes a known object volume constituting voxels, where the volume is represented by a 3D accumulator. The entire procedure contains three phases: Firstly, the volume is divided into plane cells along the Z axis. Then, each *feature point* back-projects through the voxels of the volume and the accumulator records them. Eventually, the number of rays through each voxel is checked and these rays also determine whether or not the voxel is the location of a 3D scene feature. It can be envisaged both that the performance requires enormous computer memory when more accurate localisation is needed, and the accuracy is adversely influenced if cameras are not well calibrated.

Maas (1996) has offered a solution to the problem of a fixed reference image through repeatedly assigning one image as a reference, till all images have been so selected. Range constraints are employed to confine the quantity of candidates for matching. An accumulator is used to count the hits to the current point on one image by the epipolar lines derived from the other images, without using similarity measures or relationships between neighbouring feature points. The more hits a candidate has, the more reliable it is. Moreover, the more images overlapped and applied, the more robust are the results. At least *five* images needed to be overlapped to reduce gross errors in the reported test. Nevertheless, gross errors can still exist in the case of six overlapped images due to a lack of utilisation of global quality control measures.

Applying multiple stations to cover a multi-image network has also been suggested by Maruya, Nemoto and Takashima (1992). They present a restricted system configuration consisting of multiple pairs of cameras. Each pair is processed independently, in association with a very good stereo environment. In fact, the scheme operates a two-image matching approach repeatedly to all pairs of images. Okutomi and Kanade (1993) have reported another approach to MIM.

This involves a multi-baseline stereo mounting with all cameras along one long line. The approach performs two-image matching on individual image pairs in the form of the sum of squared-difference (SSD) values and combines the sum of SSD values from all pairs. It is abundantly clear that these two methods for MIM are restricted to multi-image geometries which are not always practical.

In this paper, the proposed automatic reconstruction of a multi-ray network has the following features: 1) triangulation errors are employed as one of the sources for the relaxation probabilities used in global quality control; 2) over-parameterisation in object space matching is avoided and *ad hoc* object surface knowledge or range data (which is useful when available for 3D mensuration, e.g. El-Hakim and Beraldin, 1994) is not required; 3) a multi-image network in which images may not all be mutually overlapped, but are connected through other images and are simultaneously matched without a fixed reference image being applied; 4) the matching quality is controlled globally; 5) no approximate values for matching candidates and no interactive starting points are required, though a range constraint is desirable; and 6) there are no configuration restrictions for the camera stations.

To realise the promise of these features, three phases are conducted for the automatic construction of the multi-ray network: 1) similarity measures and epipolar curve chains are employed in conjunction with range constraints to establish initial connections between feature points and matching candidates; 2) points and their compatible neighbours construct relationships via local consistency; and 3) a multi-ray network reconstruction starts from the initial connections between feature points and matching candidates, and the relationship between neighbouring points, and then reaches an equilibrium state through a global quality controller, namely a relaxation processor.

Various experimental applications of the proposed technique have been evaluated, of which two multi-ray object reconstructions are briefly summarised in the present paper. The fields of application have covered engineering measurement (reconstruction of a rock face and determining the surface topography of a load of sand in a truck to simulate volume determination in ore trucks), industrial objects (contour verification of a wing surface profile and reconstruction of the surface of a circuit board) and natural scenes. Further applications details are provided in Fraser and Shao (1998), where performance aspects are also discussed. The performance of the multi-image matching strategy, which reaches a matching speed of close to 120 points per second for a four-image configuration (using a Pentium-200 PC platform) of Kodak DCS420 images (1524 × 1012 pixels), is very promising, as is the accuracy which can approach 0.1 pixels in a strong geometric configuration. In the following sections the major components of the MIM strategy are described and a brief account of experimental results is presented.

2. INITIAL RECONSTRUCTION OF A MULTI-RAY NETWORK

It can be envisaged that the initial reconstruction of a multi-ray image network should satisfy the following conditions: 1) homologous points should have one or more satisfied similarities; 2) the object space intersection of the homologous points must be bounded by a certain error range; 3) points to be matched in different images must lie on the corresponding

epipolar curves; and 4) each image should be able to consecutively serve as a reference image. The latter two conditions are developed in the following sub-sections.

2.1 Epipolar Curve Chains

As is well known, the coplanarity condition for two camera projective centers and an object point A with $a_1(x_1, y_1)$ and $a_2(x_2, y_2)$ being the left and right image points, is defined by

$$\begin{vmatrix} B_X & B_Y & B_Z \\ U_1 & V_1 & W_1 \\ U_2 & V_2 & W_2 \end{vmatrix} = 0 \tag{1}$$

where B_X, B_Y, B_Z are the baseline vectors on the X, Y, Z coordinate axes, respectively. U_1, V_1, W_1 are model coordinates of Point a_1 derived by a 3D coordinate transformation with a rotation matrix R which is the function of angular elements of the camera exterior orientation:

$$[U_1, V_1, W_1]^T = R \bullet [x_1, y_1, -f_1]^T$$

Similarly with a rotation matrix R', U_2, V_2, W_2 are model coordinates of Point a_2.
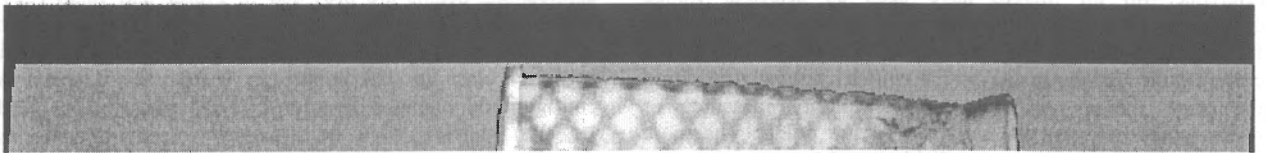
From the coplanarity formula 1, a new equation is formed:

$$\left(\begin{bmatrix} C_{00} & C_{01} & C_{02} \end{bmatrix} [x_1, y_1, -f_1]^T \begin{bmatrix} R'_{00} & R'_{01} & R'_{02} \end{bmatrix} + \right.$$

$$\begin{bmatrix} C_{10} & C_{11} & C_{12} \end{bmatrix} [x_1, y_1, -f_1]^T \begin{bmatrix} R'_{10} & R'_{11} & R'_{12} \end{bmatrix} +$$

$$\left. \begin{bmatrix} C_{20} & C_{21} & C_{22} \end{bmatrix} [x_1, y_1, -f_1]^T \begin{bmatrix} R'_{20} & R'_{21} & R'_{22} \end{bmatrix} \right)$$

$$[x_2, y_2, -f_2]^T = 0 \tag{2}$$

where
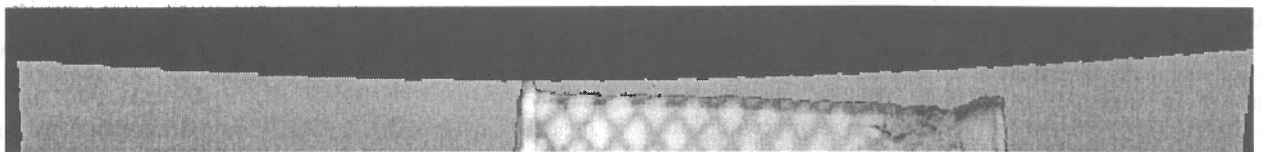
$$C_{00} = B_Y R_{20} - B_Z R_{10}$$
$$C_{01} = B_Y R_{21} - B_Z R_{11}$$
$$C_{02} = B_Y R_{22} - B_Z R_{12}$$
$$C_{10} = B_Z R_{00} - B_X R_{20}$$
$$C_{11} = B_Z R_{01} - B_X R_{21}$$
$$C_{12} = B_Z R_{02} - B_X R_{22}$$
$$C_{20} = B_X R_{10} - B_Y R_{00}$$
$$C_{21} = B_X R_{11} - B_Y R_{01}$$
$$C_{22} = B_X R_{12} - B_Y R_{02}$$

This formula is a linear epipolar line equation of the reciprocal function of either x_1 and y_1 or x_2 and y_2, in the case of known exterior orientation. However, it should be understood that lens distortion for the off-the-shelf lenses used in modern cameras employed for computer vision and close-range photogrammetry is unavoidable, and can reach 20 pixels or more towards the edges of the image format. Thus, x_1, y_1, x_2 and y_2 need non-linear correction [Fraser, 1997]. This leads to a pair of homologous points being located on an *epipolar curve* rather than on an epipolar line. Shown in Figure 1 is the situation of an epipolar curve versus a line. Elements C and R' in Eq. 2 are related to the exterior orientation of two camera stations and not to points of a stereo pair in image space. This decomposition is therefore very efficient for the computation of epipolar curves on a stereo pair of images without repetitive computation of many parameters. It should be noted that this equation can be used for epipolar curve generation for both left and right images and for the coplanarity constraint applied in image matching. However, Points (x_1, y_1) and (x_2, y_2) must be matched to elements C and R', respectively. If Points (x_1, y_1) and (x_2, y_2) both are in the left image, then R' must be the rotation matrix of the left image. Otherwise, R' must be the rotation matrix of the right image.

From the analysis above, we know that a 'right-image' point constructs a corresponding epipolar curve through a 'left-image' point, and generally one image point in an image generates $N-1$ epipolar curves on the other $N-1$ overlapping images. So, N overlapped images generate a total of $N \times (N-1)$ epipolar curves for one object point. These epipolar curves constitute an epipolar curve chain.

a. The epipolar line is re-imaged from the border of an image *without* lens distortion correction.

b. The epipolar curve demonstrates where the homologous points should lie when radial lens distortion is considered.

Fig. 1: Epipolar lines and curve.

On the epipolar curve chain, one image point may have more than one candidate on the other images due to incompleteness of camera calibration and/or orientation, errors of feature point location [Foerstner, 1986] and repetition of point similarity. The first two concerns give rise to triangulation errors. These triangulation errors lead to *discrepancy ambiguities* which indicate that a point in one image matches to a number of points of a group on the other images. These group points, which of course also satisfy similarity criteria, are neighbours to a potentially homologous point. The repetition of point similarity causes *repetition ambiguities* indicating that there are points in other groups matching to the point a on the first image, because of the same similarity, and certainly also satisfying the triangulation error constraint.

Shown in Figure 2 are two such types of ambiguities. In the figure, A_1 is a true object point. A_2, very close to A_1, indicates the discrepancy ambiguity, while A_3, far away from A_1, represents the repetition ambiguity. Obviously if a true object point is approximately known, the repetition ambiguity can be eliminated by using local consistency checks, whilst the discrepancy ambiguity is able to be removed through multi-ray triangulation residuals and similarities. However, in the absence of any object surface knowledge the elimination of the two ambiguities needs to be taken into account in combination. The details of this procedure will be explained in a later section.
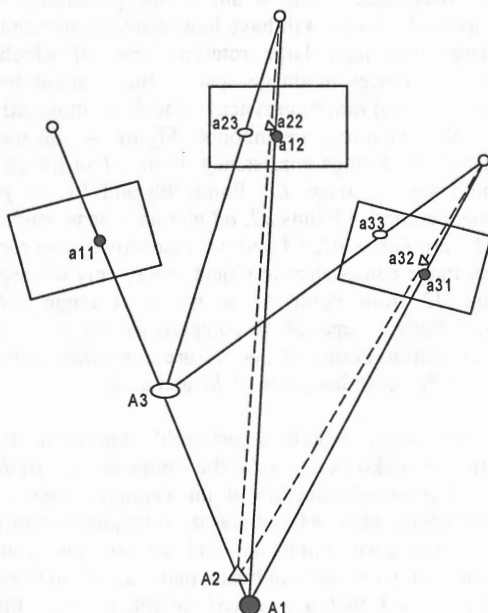
Fig. 2: One image point may have multiple nodes in the multi-ray network. The node portrayed by solid circles is true. Indicated by open ellipses is a repetition ambiguity, while represented by triangles is a discrepancy ambiguity.

2.2 Consecutive Consideration of All Images

For the sake of simplicity, suppose there are four images to be matched and one point in the first image is known. The consecutive procedure of the network construction involves several phases. First of all, there is a search of all candidates on the epipolar curve in the second image. Then, three dimensional coordinates are computed between the point in Image 1 and the candidates in Image 2. Those which are out of the depth range

set up in a range constraint are then filtered out. One candidate among those remaining is then selected, and the three dimensional coordinates of the candidate are back-projected into the image planes of the remaining images through the collinearity equations. The image coordinates of points in the other images are then derived, and neighbourhoods are examined to find candidates according to the epipolar geometric and object space constraints. When all points in Image 1 are processed, points in the next image are considered and search candidates in the remaining images are selected. This ensures that every point in every image has the opportunity to seek candidates. When all points in the images are complete, those which have constructed the nodes of the multi-ray network are marked.

Through an overall extension from an individual image point and its candidate image points and objects, as shown in Figure 2, to all feature points in an entire multi-image block, an initial multi-ray network can be constructed as indicated in Figure 3. In this figure, one object point may have more than two imaging rays. Open circles and ellipses in the figure represent ambiguous image points and virtual object points, respectively. Virtual rays linking the open circles and ellipses are indicated by dashed lines and the solid circles and ellipses are real homologous image and object points, which are connected by solid lines. Some images are not overlapped, but are connected through other images.

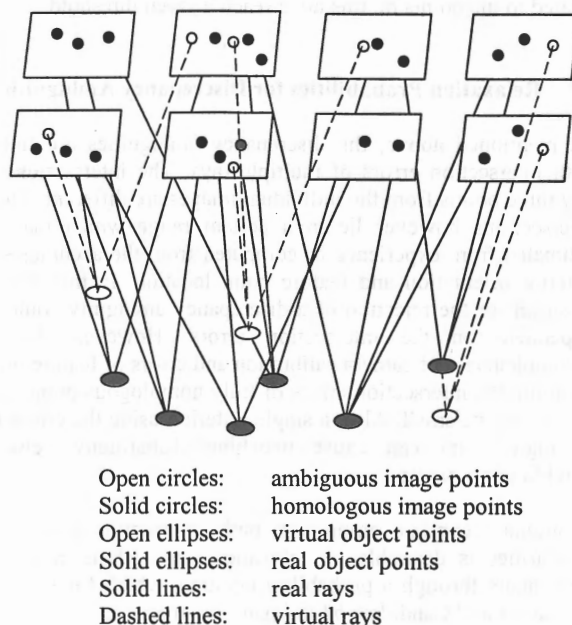| Open circles: | ambiguous image points |
Solid circles:	homologous image points
Open ellipses:	virtual object points
Solid ellipses:	real object points
Solid lines:	real rays
Dashed lines:	virtual rays

Fig. 3: An initial construction of a multi-ray network.

Each feature point, as described above, may have several ambiguous points. To eliminate ambiguities, a relationship among neighbouring feature points in the same image, with their corresponding object points, is needed for a global quality control check. This aspect is described in the next section.

3. Global Quality Control

As has been discussed, there are two types of matching ambiguities. To eliminate the two ambiguities, two sets of compatibility functions in a relaxation process are introduced.

This is a popular optimisation algorithm which has previously been adopted in a three-line CCD image matching method [Wu and Murai, 1997]. One set of functions is linked with the triangulation intersection errors of multiple rays, while the other is related to local consistency with neighbouring nodes. Then, two relaxation probabilities derived from the two sets of compatibility functions are combined together. Assuming a point $a1$ in image i and a candidate $b1$ in image j are pre-matched, the symbolic expression for the probability combination is

$$P_{ij} = P'_{ij} + \lambda \times P''_{ij} \qquad (3)$$

where P'_{ij} and P''_{ij} are two normalised discrete probabilities relevant to the first and second types of compatibility functions for Point $a1$ to Candidate $b1$, and λ is a controllable scaling parameter governing the respective contributions of the two types of probabilities. Then an iteration, e.g. from the iteration number k to $k+1$ is applied as

$$P^{k+1}_{ij} = A + B \times P^k_{ij} \qquad (4)$$

where A and B are the coefficients controlling convergence speed. A multi-ray network node is then accepted only if all probabilities P_{ij} ($i, j \in N$, $i \neq j$ with N representing the number of overlapped images of the node in the multi-ray network) related to the points on this node reach a given threshold.

3.1 Relaxation Probabilities for Discrepancy Ambiguities

As mentioned above, the discrepancy ambiguities are linked with intersection errors of multiple rays. The intersections of any three points from the individual images are different. These intersections however lie in a certain range which may be estimated from experience or computed from the accuracies of exterior orientation and feature point location. In this case, a criterion for the rejection of a discrepancy ambiguity could be dependent on the intersection errors. However, due to incompleteness of camera calibration and errors of feature point location, the intersection errors of truly homologous points will not always be small. Also, a single criterion using the errors for a single point can cause matching disharmony between neighbouring pixels.

A global technique employing both intersection errors and similarities is desirable. A relaxation approach is employed here, again through a probability iteration, which for Point $a1$ in image i and Candidate $b1$ in image j is given as:

$$P'_{ij} = P_{\Sigma} \times f(e_{ij}) \qquad (5)$$

with

$$f(e_{ij}) = \exp(\frac{1}{e_{ij} + c}), \ \frac{1}{e_{ij} + c}, \ \text{or} \ \frac{1}{\sqrt{e_{ij} + c}}$$

and

$$P_{\Sigma} = \sum_{k \in N, k \neq i, j} (P_{jk} \times f(e_{jk}))$$

Here, P_{ij} are the first type of probabilities against the discrepancy ambiguities and $f(e_{ij})$ are the multiple options of the functions of the intersection errors e_{ij} derived from the current points in image i to j. Similarly $f(e_{jk})$ are the functions of the intersection errors e_{jk} derived from the related points in images j and k ($k \in N$). These points must be in the same epipolar curve chain. P_{Σ} is the total weighted probability supported from all P_{jk} which are the probabilities of the points in the current iteration for image j to k, and c is a small constant for prevention of computational overflow. The P_{jk} values in the first iteration are created from similarity measures. The physical meaning of P_{ij} is that the smaller the triangulation errors from the other rays on the same epipolar curve chain, and the more imaging rays, the greater the support for the current candidate. This is a global network consideration for the determination of matching points.

3.2 Relaxation Probabilities for Repetition Ambiguities

As usual, the repetition ambiguities are removed through local consistency checks within a neighbourhood. Removal of ambiguities using alternative approaches has often been achieved in image space, where consistent disparity can be used for near standard binocular feature-based matching. In contrast, disambiguation in our strategy is realised in object space rather than in image space. This is due to the possibility that the optical axes of cameras will have large convergence angles and the images may have large rotation, both of which cause disparity differences in image space which cannot be easily compared. A local range consistency check is employed for the capture of *compatible* neighbours. Figure 4 illustrates the principle of local range consistency. Point $a1$ in Image $L1$ has two candidates in Image $L2$: Points $b0$ and $b1$. Its *physical* neighbours comprise Points $a2$, $a3$ and $a4$ whose candidates in Image $L2$ are Points $b2$, $b3$ and $b4$, respectively. According to the local range consistency in object space, only the separation of Point $A2$ from Point $A1$ is within a range difference tolerance, while $A3$ and $A4$, in comparison with $A1$, are out of range. Therefore, Points $a1$ and $a2$ are *compatible* neighbours in terms of the candidate pairs $a1$-$b1$ and $a2$-$b2$.

On the other hand, no point is compatible with Point $A0$, ie. no compatible neighbours exists for the candidate pair $a1$-$b0$. This leads to a potential selection of the candidate pair $a1$-$b1$ as matched points. Also, $A3$ and $A4$ are mutually within a range difference tolerance. Points $a3$ and $a4$ are thus compatible neighbours in terms of candidate pairs $a3$-$b3$ and $a4$-$b4$. It should be noted that a *physical* neighbour may not be a *compatible* neighbour, but, a compatible neighbour must be a physical neighbour. Also, a compatible neighbour itself does not have any meaning. It is meaningful only in terms of certain candidate pairs, e.g. in Figure 4 Points $a1$ and $a2$ are compatible neighbours in terms of the candidate pairs $a1$-$b1$ and $a2$-$b2$.

If the object surfaces being reconstructed are fairly smooth, local range consistency is replaced by local slope consistency for the check of compatible neighbours. This is due to the fact that the former tolerates a certain discontinuity of object surfaces, while the latter is able to control gross errors, though they may only be few in the multiple-ray case. Applying this principle to every feature point, a compatible relationship among neighbours is established, as illustrated in Figure 5.
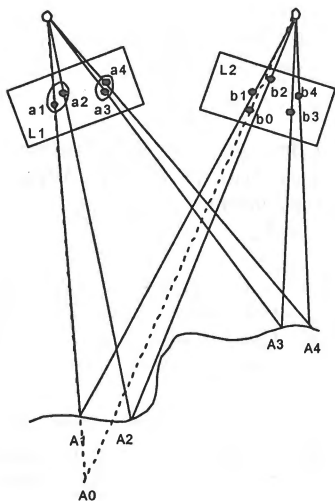
Fig. 4: The circled points in the image plane *L1* are *compatible* neighbours obtained by a local range consistency check.
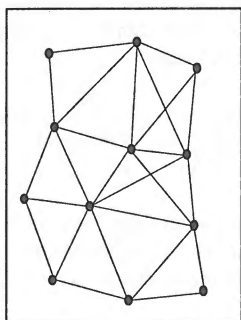

Fig. 5: A relationship is woven among neighbouring feature points of the same image, through local consistency. Dots stand for objects and lines for linkages to the objects.

From the compatibility relationship, local mutual consistency reinforces the repetition probabilities from compatible neighbouring points a:

$$P_{ij}^{"} = \sum_{a \in R} P_{ij}$$

where R is a local region, in which a satisfies the local consistency condition in image i to image j. For instance, again in Figure 4, for Point $a1$ on Image $L1$ to Image $L2$ the relaxation probability for the repetition ambiguity is $\sum P_{L1L2} = P(a2 - b2)$, which is the current probability of the candidate pair $a2$-$b2$ on Image $L1$ to $L2$. The physical meaning of $P_{ij}^{"}$ is that the more consistent neighbours and the high relaxation probabilities arising on the same image, the more support for the current candidate pair.

4. EXPERIMENTS

In order to ascertain the computation time and accuracy of the multi-ray network reconstruction, the proposed approach was evaluated using a digital image network acquired with a Kodak DCS420 still video camera. The first object investigated comprised a car door with a random projected line pattern, as shown in Figure 6. The time and accuracy evaluations of the matching approach were carried out using a configuration of four convergent images.
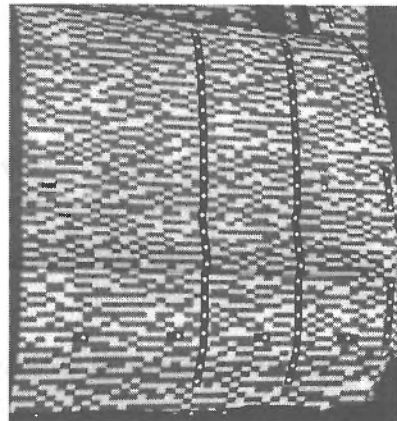

Fig. 6: Car door with a projected random line pattern.

Given the impact of factors such as image content, image quality, the number of images and disparity differences, the achieved matching speed of 115 3D coordinate points per second should be viewed as indicative only. This performance was obtained in a Windows 95 environment of Microsoft C++, with the PC processor being a Pentium-200. Since the car door surface is rather smooth, the Z coordinate accuracy was of special concern. RMS 'height' errors were found to be 0.08 mm, which is equivalent to 0.1 pixels when projected back to image coordinates. Shown in Figure 7 is a digital surface model (DSM) resulting from the multi-ray network, which indicates a smooth (accurate) surface reconstruction.
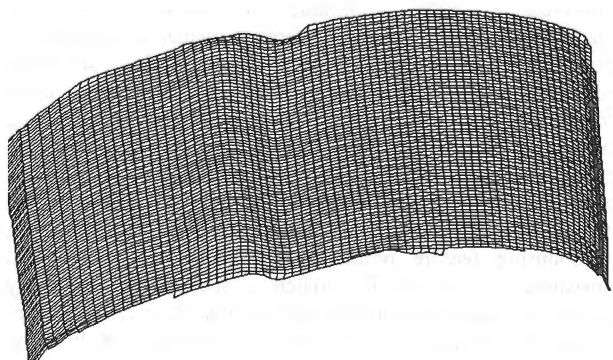

Fig. 7: Derived DSM of the car door.

A second application involved the reconstruction of a natural scene, namely a rock face. Shown in Figure 8 is the camera station configuration of the multi-ray network for the rock face survey. In the figure, the number of images, camera positions and camera convergence angles are indicative only. Actually, 14 images with *arbitrary convergence angles* were employed. The 3D reconstruction map shown in Figure 9 proved to be of high accuracy, again around 0.1 pixels, which illustrated that the proposed technique can be usefully applied to natural scenes. Further testing of the method is ongoing, and additional experimental results are presented in Fraser and Shao (1998).
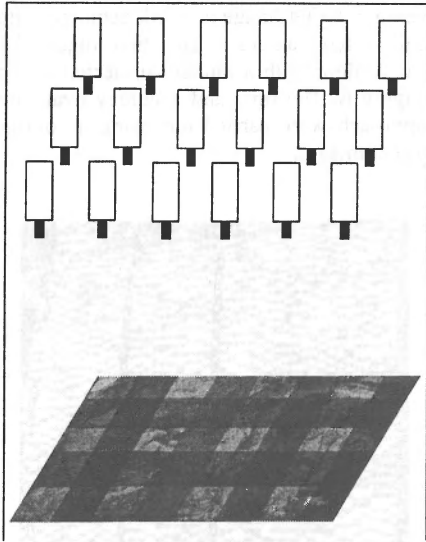
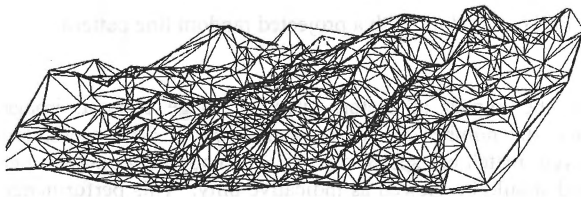Fig. 8: The indicative configuration of the multi-ray rock-face network.

Fig. 9: The DSM of the measured rock face reconstructed via the multi-ray network.

5. CONCLUSIONS

This paper has described automatic reconstruction of a digital multi-ray photogrammetric network through use of a novel feature-based MIM technique in which consecutive consideration of all images as reference images is proposed. A combined utilisation of epipolar curve chains, similarity measures and range constraints leads to the initial reconstruction of the multi-ray network. A global matching quality control using a relaxation process finally produces a refined multi-ray network reconstruction which employs a check for correspondence ambiguities. In the check, the creation of geometric relationships among compatible, neighbouring feature points in the same image via local consistency is verified. The matching speed in the multi-ray network reconstruction in the case of four close-range images reaches 115 3D points per second on a Pentium-200 PC. The resulting accuracy reaches 0.1 pixels. This approach can thus be employed for both high accuracy vision metrology and accurate initial value acquisition in very precise least-squares matching applications.

6. REFERENCES

Chiou, R.N., Chen, C.H., Hung, K.C. and Lee, J.Y., 1995. The Optimal Camera Geometry and Performance Analysis of a Trinocular Vision System. *IEEE Trans. Systems, Man and Cybernetics*, 25(8): 1207-1220.

Collins, R., 1996. A Space-Sweep Approach to True Multi-Image Matching. *Proceeding of 1996 IEEE Computer Society Conference on Pattern Recognition*, San Francisco, CA, pp. 358-363.

El-Hakim, S. and Beraldin, J.-A., 1994. On the Integration of Range and Intensity Data to Improve Vision-Based Three Dimensional Measurements. *Proceedings of SPIE 2350, Videometrics III*: 306-321.

Faugeras, O., Lustman, F., and Toscani, G., 1987. Motion and Structure from Motion from Point and Line Matches. *Proceeding of 1st International Conference on Computer Vision*. June 8-11, London, pp. 25-34.

Foerstner, W., 1986. A feature Based Correspondence Algorithm for Image Matching. *Proceeding of the Symposium on From Analytical to Digital*. Rovaniemi, Finland, August 19-22, pp.150-166.

Fraser, C., 1997. Digital Camera Self-calibration. *ISPRS International Journal of Photogrammetry and Remote Sensing*, 52: 1449-159.

Fraser, C. and Shao, J., 1998. Application of a Multi-Image Matching Scheme for Close-Range Photogrammetry. *Submitted to Geomatics Research Australasia*.

Gruen, A. and Baltsavias, E., 1988. Geometrically Constrained Multi-photo Matching. *Photogrammetric Engineering and Remote Sensing*, 54(5): 633-641.

Heipke, C., 1992. A Global Approach for Least Squares Image Matching and Surface Reconstruction in Object Space. *Photogrammetric Engineering and Remote Sensing*, 58(3): 317-323.

Ito, M. and Ishii, A., 1986. Three View Stereo Vision. *IEEE Trans. on Pattern Recognition and Machine Intelligence*, 8(4): 524-532.

Maruya, M., Nemoto, K. and Takashima, Y., 1992. Texture Based 3-D Shape Reconstruction from Multiple Stereo Images. *Proceeding of 11th IAPR International Conference on Pattern Recognition*, The Hague, Netherlands, 30 August- 3 September, pp137-140.

Maas, H.-G., 1996. Automatic DEM Generation by Multi-Image Feature Based Matching. *International Archives of Photogrammetry and Remote Sensing*, 31(B3): 484-489.

Okutomi, M. and Kanade, T., 1993. A Multi-Baseline Stereo. *IEEE Trans. on Pattern Recognition and Machine Intelligence*, 15(4): 353-363.

Shibasaki, R. and Murai, S., 1988. Improvement of Mapping Accuracy by Applying Triplet Matching to SPOT Imagery. *International Archives of Photogrammetry and Remote Sensing*, 27(B4): 264-273.

Wu, X. and Murai, S., 1997. Image Matching Using a Three Line Scanner. *ISPRS Journal of Photogrammetry and Remote Sensing*, 52: 20-32.